AIAA JOURNAL
Vol. 46, No. 6, June 2008

Orthogonal Blade-Vortex Interaction on a Helicopter Tail Rotor

Antonio Filippone* and Imran Afgan†
University of Manchester, Manchester, England M60 1QD, United Kingdom

DOI: 10.2514/1.32690

The orthogonal blade-vortex interaction has been simulated using unsteady Reynolds-averaged Navier–Stokes equations with turbulence closure equations. The cases investigated are relative to an interaction between a lifting blade at a high angle of attack and an orthogonal vortex that travels either head-on or at 45 deg to the leading edge. The numerical simulations have been performed at a Reynolds number of $Re = 1.85 \times 10^5$ and a vortex Reynolds number of $Re_v = 10^5$. The impact parameter is equal to 8, which places the interaction in the weak vortex regime. The initial axial velocity of the vortex is zero, but as the vortex travels a self-induced velocity causes the vortex to move axially well before the impact on the blade. The analysis is carried out on the vortex dynamics and on the blade aerodynamics. The data investigated include the behavior of the pressure field as the vortex advances, the distribution of vorticity, the interaction of the vortex with the blade and the wake, the flow separation at the blade surface, and the path lines of the flow. A comparison between the case of straight and oblique blade-vortex interaction indicates that the blade-vortex interaction pressure peak is less severe in the latter case. A comparison is also made for the corresponding aerodynamic force coefficients (lift and drag and normal force).

Nomenclature

A	=	vortex axial flow parameter
C_D	=	drag coefficient
C_L	=	lift coefficient
C_n	=	normal force coefficient
C_{n_o}	=	steady-state C_n
C_p	=	pressure coefficient, $(p - p_\infty)/\rho U^2/2$
c	=	blade chord
I	=	impact parameter
L	=	lift force
p	=	pressure
$\mathbf{r}$	=	radial vector
R	=	blade radius
Re	=	Reynolds number
Re_v	=	vortex Reynolds number, $U_r c/\nu$
T	=	rotor thrust
t	=	thickness of the blade section
$\mathbf{U}_r$	=	relative velocity
U_s	=	vortex self-induced velocity
U_{tip}	=	tip speed
$\mathbf{U}_v$	=	convection velocity of vortex
U_∞	=	flight speed
$\bar{w}$	=	downwash velocity of a rotor
w_o	=	swirl velocity at the vortex core
x, y, z	=	Cartesian coordinate system
α	=	angle of attack
Γ	=	vortex circulation
κ	=	lift–curve slope factor
μ	=	blade's advance ratio, U_∞/U_{tip}
ν	=	fluid viscosity
σ_o	=	vortex core
Ω	=	rotor speed
$\boldsymbol{\omega}$	=	vorticity vector

Received 8 June 2007; revision received 19 September 2007; accepted for publication 12 March 2008.

*Lecturer, School of Mechanical, Aerospace and Civil Engineering, George Begg Building, Post Office Box 88; a.filippone@manchester.ac.uk. Senior Member AIAA.

†Doctoral Student, School of Mechanical, Aerospace and Civil Engineering.

I. Introduction

THE interaction between a vortex and a rotating blade is a common fluid dynamic problem in helicopters. A typical case involves a quartering flight, for example, a situation in which the helicopter has a strong side wind component. In this situation, tip vortices released by the main rotor blades travel toward the tail rotor disk. The interaction depends on the actual flight condition, on the geometry of the tail rotor, and on the sense of rotation. More specifically, in helicopter operations there can be interaction between the main rotor's tip vortex and a tail rotor blade, interaction between a vortex and the tail rotor's wake, or interaction between the tail rotor's own tip vortex and the incoming tail rotor blade. Finally, there is the interaction between the tip vortex of the main rotor blades and the fuselage or the tail boom, and the interaction between the tail surfaces and the tail rotor. However, the problem is of more general importance, because it also occurs on aircraft and ship propellers.

The blade-vortex interaction (BVI) takes place in a variety of ways. The encounter can be characterized in terms of reciprocal direction: parallel, oblique, and orthogonal, depending on the axes of the blade and the vortex. These cases are shown in Fig. 1. Orthogonal BVI is to be understood as the interaction between a vertical vortex and a spanwise blade. The interaction between a streamwise vortex and a spanwise blade is also orthogonal, Fig. 2, but it is called perpendicular, instead. The orthogonal BVI is the only case among the basic cases shown in Figs. 1 and 2 that features a vortex cut through the blade. The other cases are characterized by vortices traveling at a short distance from the blade, without direct impact. The orthogonal BVI investigated in this research is a considerably more complex fluid dynamic problem, because the vortex dynamics and the blade's response depend on several flow parameters.

The interaction problem can be extended to the case of a convecting vortex encountering the wake of a rotor blade. This interaction is dependent on whether the impact is at a stage when the tip vortex is in the roll-up process or is fully developed. In the latter case it has only marginal effect on the aerodynamic and aeroacoustic responses of the blade.

All the cases described involve impulsive aerodynamic loads that inevitably lead to impulsive pressures and hence noise. In fact, sound generation from the BVI has been a long-standing problem in helicopter aerodynamics (see Leverton et al. [1]) and the main motivator for research in this field. Much of the initial research was aimed at assessing methods for the reduction of tail rotor noise for the purpose of flight certification. For example, Cary [2] described oil flow and stroboscopic visualization of the BVI, but also the sound pressure level response of the BVI encounter.

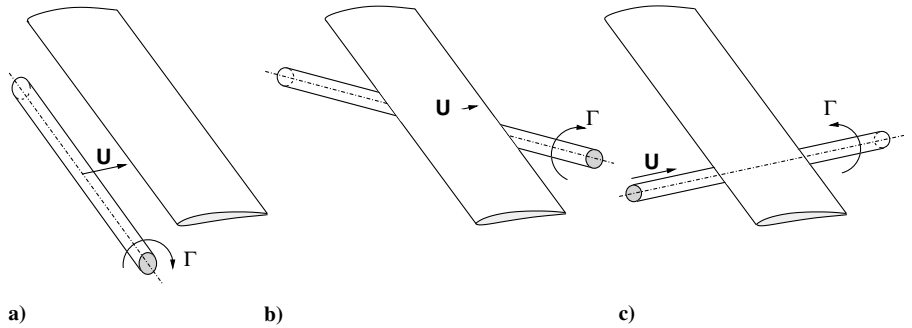

Fig. 1 Examples of blade-vortex interaction.

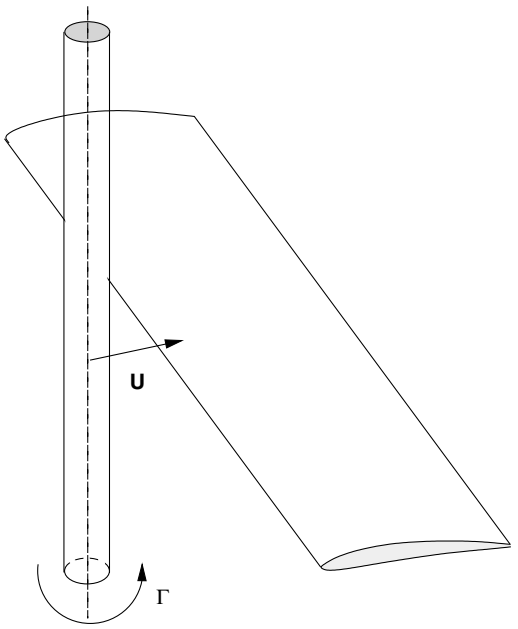

Fig. 2 Orthogonal BVI.

The other aspects of the BVI include impulsive aerodynamic loads, mechanical vibration, and structural fatigue. The aerodynamic aspect of the BVI that has been investigated in more detail in recent years is the interaction between the tip vortex released by one blade of the main rotor and the incoming blade. However, the event often occurs on the tail rotor. If the BVI is caused by vortices in short sequence (high frequency), the problem is further complicated, because the blade has to respond to a new loading before the current BVI loading has subsided. As the vortex departs from the blade at the trailing edge, it interacts with the wake (shear layer). The process is sometimes called blade-wake interaction (BWI), and is by itself another source of acoustic excitation, as shown in the case of parallel BWI (Wittmer et al. [3,4]). The interaction between the vortex and a large surface, such as the fuselage, is similar to the interaction with the orthogonal BVI on a thin blade, but an essential aspect is the strong deformation of the vortex ahead of the impact, mostly as a result of the relationship between the size of the vortex core and the thickness of the body [5–7].

The main features of the vortex are its core size, the circulation (or swirl velocity), and the axial velocity component. Measurements shown by Bhagwat and Leishman [8] on a tip vortex of a helicopter rotor indicate that the swirl velocity is maximum at the radius of the vortex core; this velocity tends rapidly to zero approaching the axis of the vortex. Furthermore, there is a small axial velocity component inside the vortex, with its maximum at the axis. This velocity component tends to zero toward the edge of the core. Doolan et al. [9] contended that when the vortex is cut by the blade, this axial velocity component is inhibited. This event forces the vortex with the axial velocity component pointing toward the blade surface to expand. By contrast, the separated vortex core on the opposite side of the blade tends to become thinner as a consequence of having an axial velocity component away from the blade's surface. Marshall and Krishnamoorthy [10] performed detailed experimental investigations that highlighted the role of the axial velocity component in the vortex core. It was shown that for cases of low-speed impact the boundary layer is ejected from the blade's surface. Lee et al. [11] studied in detail the flowfield inside and around the vortex by performing inviscid computations of a BVI with a thin plate and arrived at the same conclusion. Furthermore, they linked the pressure suction peak to the direction of the axial velocity on the vortex core. In a case of a vortex core with an axial velocity component away from the plate, the suction peak persists and the vortex core shrinks.

A review of the orthogonal BVI state of the art was published by Coton et al. [12], who reported both the experimental and computational results available. The group at Glasgow University has published fundamental results for the understanding of the mechanism of the vortex cutting by a rotating blade. For example, Doolan et al. [9], Green et al. [13], and Wang et al. [14] performed BVI experiments in which a rotor blade operated inside a wind tunnel. In the experiments described in the latter paper vortices were generated by the rotor and convected downstream, where they impacted on a blade. These experiments highlighted the fact that the pressure peaks on the blade decreased by moving away from the vortex. Rapid changes in the normal forces were detected as the vortex impacted the blade. Additional experiments were performed by Krishnamoorthy and Marshall [15] with laser-induced fluorescence methods. These experiments addressed the BVI problem in the strong vortex regime. When the incoming vortex interacts strongly with the blades boundary layer, it causes separation, ejection of vorticity, and the creation of secondary vortices; these vortices interact with the incoming vortex core. A phenomenon of particular interest in the parametric space investigated by these authors is the dynamics of the vortex core when it is surrounded by vortex rings created by the interaction.

Most of the computational work on BVI is on the acoustic response. Aerodynamic investigations have been performed by Yin and Ahmed [16], who used a three-dimensional panel method with a free wake, coupled with an independent aeroacoustic solver, based on the Ffwocs-Williams and Hawking equation.

Marshall and Grant [17] used the vorticity transport equation for the solution of a BVI problem in which a vortex ring (or core) penetrates into a planar blade. It was argued that because the case did not involve a strong interaction between the vortex and the boundary layer, the inviscid flow model would suffice in providing a sufficiently accurate flow model. These authors further analyzed the blade pressures by solving integral equations on the blade surface and concluded that the pressure suction is proportional to the square of the vortex circulation. Earlier, Howe [18] concluded that also the dipole strength of the acoustic signal is proportional to the square of the vortex circulation. However, this analysis considered only a two-dimensional problem past a nonlifting airfoil.

Marshall [19] derived a theory for long-wave motion of thin vortex filaments and derived an expression for the response of the blade during cutting. This expression relates the blade loading to the ratio

between the vortex core radii above and below the blade. The method was then applied to the calculation of blade response (Marshall and Yalamanchili [20]) with a variety of thicknesses and angles of attack.

Finally, Liu and Marshall [21] presented one of the very few cases documented in the literature of a vortex cutting by a blade in a viscous flow. The cases examined were limited to low Reynolds numbers ($Re < 2000$), and the interaction was with a nonlifting blade (NACA 0012 section at zero angle of attack). However, these authors reported a wide variety of cases, some of which involved axial flow in the vortex core.

Thus, the present study arises from the limited computational data available in the technical literature on orthogonal BVI and from the need to simulate the BVI in a realistic rotor environment. The study proceeds through an analysis of the tail rotor environment, then through a simplified computational model of the BVI. The results address two aspects: the time-dependent loading on the blade and the fluid dynamics of the vortex in all the encounter phases with the blade. Two cases are considered: 1) straight (head-on) impact and 2) impact with an approach angle of 45 deg. Section II is a discussion of the tail rotor environment and the type of vortex regimes that are routinely encountered in helicopter operations. Section III contains a description of the computational model, including the vortex core, and Sec. IV is a critical discussion of the results obtained.

II. Analysis of Tail Rotor Environment

The case of interest is the aerodynamic effect of a tip vortex released by the main rotor passing through the rotor disk of a tail rotor. The process is indicated in Fig. 3. This graphic shows the vortex path inferred from pressure readings and particle-image velocimetry [22]. Both at the forward climb and level flight condition the vortex travels through the rotor disk, and thus encounters a rotating blade that can penetrate at various angles. The cases shown in Fig. 3 are relative to a helicopter in full configuration. Details of the experimental setup are given by Langer et al. [22]. In reality, a number of complicating factors intervene. One of these is the unsteady effect created by the interference of the vertical fin. Another effect is the high frequency of interaction, due to the combination of blade numbers in the main and tail rotor. Because the tail rotor speed is 5 times the main rotor speed, there are five full cycles in the aerodynamic loads for each rotation of the tail rotor. The isolation of the effect of the vertical fin has proved to be difficult.

The model proposed in the following discussion relies on a single blade, whose flow is considered free of all interference. Furthermore, the sequence of interactions is spaced such that a vortex has passed through the blade before another one impacts. The condition for this to occur is that the time between interactions is much greater than c/U, where U is the average relative velocity between blade and vortex.

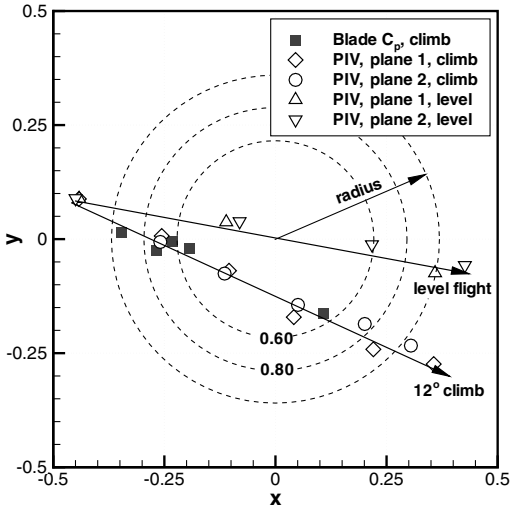

Fig. 3 Wind-tunnel data of tail rotor BVI. Vortex axis normal to the page. PIV = particle image velocimetry.

Marshall and Krishnamoorthy [10] summarized the BVI phenomenon as dependent on three nondimensional physical parameters. One is the impact parameter $I = 2\pi\sigma_o U/\Gamma$, with σ_o the radius of the vortex core. The impact parameter is the ratio between the relative velocity U and the vortex swirl velocity component at the vortex core, $\Gamma/2\pi\sigma_o$. For a given vortex core dimension, a large axial vorticity (or swirl velocity), relative to the impact speed leads to a low impact parameter. This is a case of a "vortex" dominated interaction. Furthermore, one can define the nondimensional axial flow parameter (for a vortex with an axial velocity component at the core), $A = 2\pi\sigma_o w_o/\Gamma$, where w_o is the maximum axial velocity in the vortex core. Finally, the thickness parameter is the ratio between the wing thickness and the vortex core, t/σ_o.

A further aspect of interest in the axial velocity parameter is given by the Lundgren–Ashurst criterion [23] that was derived for a vortex with constant axial velocity and vorticity in the vortex core. The criterion establishes a limit in the axial velocity parameter ($A = \sqrt{2}$), such that a value of A below this limit would yield a subcritical flow. This is a flow in which the wave propagation caused by the BVI propagates both upstream (compression wave) and downstream (expansion wave). By contrast, in a supercritical flow ($A > \sqrt{2}$), the waves can only propagate downstream. Because the present analysis is limited to the case $A = 0$ (at the initial stage), the flow is subcritical, and the effects of the BVI are expected to propagate in both directions. This problem is further described by Marshall and Krishnamoorthy [10].

Marshall and Krishnamoorthy reported that for $t/\sigma_o < 1$ two vortex regimes are clearly identified. When the impact parameter $I > 0.25$ (moderate impact speed), the vortex is too weak to cause boundary layer separation on the blade before impact occurs. At lower impact parameters, $I < 0.1$ (high swirl velocity) it was found that vorticity is ejected from the boundary layer before the impact, with consequent separation. This case is characterized by the interaction between the vorticity ejected by the boundary layer and the vortex itself. At values of the impact parameter between these two extremes, boundary layer separation and interaction between incoming vortex and surface vorticity may coexist. The case with $I < 0.1$ is called strong vortex regime; by contrast, a BVI with a relatively large impact parameter is a weak vortex regime.

A rough estimate of some of these parameters can be given for the particular application to helicopter rotors. Consider first the interaction between the tip vortex released by the main rotor blade and the tail rotor blade. Abstracting from strong three-dimensional effects (spanwise flows), the bound vortex circulation of a blade section is

$$\Gamma = \frac{L}{\rho U_{\text{tip}}} = \pi\alpha c U_{\text{tip}} \tag{1}$$

In fact, the flow in the tip region has a spanwise component that would reduce the bound circulation from the theoretical 2π to a somewhat lower value. This effect can be taken into account by a corrected lift–curve slope $2\kappa\pi$. Hence, the impact parameter becomes

$$I = \frac{2\pi\sigma_o U}{\Gamma} = \frac{2\sigma_o}{\kappa\alpha c}\left(\frac{U}{U_{\text{tip}}}\right) \tag{2}$$

where U is the magnitude of the impact velocity, and α must be given in radians. Typical angles of attack at the blade tips are 2 to 5 deg, increasing to 10 deg for highly loaded rotors. The size of the vortex core is $\sigma_o/c \simeq 0.2$. Relative to a tail rotor blade chord, an approximate value is $\sigma_o/c \simeq 0.4$. A reasonable value for the corrective lift–curve slope in the vicinity of a blade tip is $\kappa \simeq 0.8$, which leads to an impact factor of the order of $I \simeq 10(U/U_{\text{tip}})$. The calculation of the velocity ratio U/U_{tip} is not straightforward, because it depends on the flight conditions and on the rotational speed of the tail rotor. Nevertheless, it is possible to calculate its order of magnitude. By approximating further, consider that the vortex "descends" at the same speed as the main rotor's downwash, which is

$$\bar{w} = \left(\frac{T}{2\rho\pi R^2}\right)^{1/2} \tag{3}$$

where T is the rotor thrust and R is the rotor radius. Note, however, that this vortex generally has a strong axial component of the velocity and will impact on the tail rotor blade while translating on itself. A tail rotor may rotate either toward the downwash or against it. Therefore, the impact velocity would be

$$U \sim U_{\text{tr}} \pm \bar{w} \tag{4}$$

where U_{tr} is the local rotational speed. If the impact is at the tip of the tail rotor, then

$$\frac{U}{U_{\text{tip}}} \sim \frac{U_{\text{tr}} \pm \bar{w}}{U_{\text{mr}}} \sim \left(\frac{\Omega_{\text{tr}}}{\Omega_{\text{mr}}}\right)\left(\frac{R_{\text{tr}}}{R_{\text{mr}}}\right) \pm \frac{\bar{w}}{U_{\text{mr}}} \tag{5}$$

The analysis of several rotorcraft indicates that average values are $\Omega_{\text{tr}}/\Omega_{\text{mr}} \sim 5$, $R_{\text{tr}}/R_{\text{mr}} \sim 0.15$ to 0.20. Hence,

$$\frac{U}{U_{\text{tip}}} \sim 1 \pm \frac{\bar{w}}{\Omega R} \tag{6}$$

with $\bar{w}/\Omega R < 0.1$. Equation (6) does not include the effects of the self-induced velocity by the vortex, $U_s = k\Gamma/4\pi R$, which is always small (k is a parameter, $k = \ell_n[8R/\sigma_o] - 0.25$). Hence, we conclude that the impact parameter for this flight condition of the order of 10 and the BVI is clearly in the weak vortex regime.

The interaction between the main rotor tip vortex and a tail surface is in a different regime. In fact, for operational cases where the interaction can be considered orthogonal, the impact velocity is of the order of the advance ratio of the main rotor, $\mu \sim U_\infty/U_{\text{tip}}$

$$\frac{U}{U_{\text{tip}}} \sim \frac{(U_\infty^2 + \bar{w}^2)^{1/2}}{U_{\text{tip}}} \sim \left(\frac{U_\infty}{U_{\text{tip}}}\right) \simeq \mu \tag{7}$$

where U_∞ is the flight speed of the helicopter. At low advance ratios, the impact will be in the strong vortex regime, in-line with the analysis provided by Krishnamoorthy and Marshall [15]. Note that in this case the chord c to be used in Eq. (2) is the average chord of the tail surface, which is considerably larger than the tail rotor blade.

This brief discussion serves to point out that the flow environment of the orthogonal BVI on a helicopter encompasses all the vortex regimes, depending on the operational conditions and on the type of interaction.

The cases discussed further in this study refer to a vortex having a strength $\Gamma = 4.5$, vortex core radius $\sigma_o = 0.045$, and a normal impact velocity $U = 36$ m/s. This leads to $I \simeq 8$, a value of the same order as the one discussed previously for the main rotor and tail rotor BVI. The value of the circulation was inferred from the aerodynamic conditions of a one-fourth–scale rotor model rotating at 5600 rpm. The thickness ratio is $t/\sigma_o \simeq 0.165$.

III. Computational Model

The computational domain is a regular box, as shown in Fig. 4, with periodic boundary conditions. The streamwise axis is x; the spanwise axis is called z. There is an inlet boundary condition upstream (specified inflow), an outlet condition downstream, periodic boundary conditions at the x–y planes (blade tips) and on the x–z planes (orthogonal to the axis of the vortex). Thus, the tip flow is not simulated. These conditions are similar to those used by Liu and Marshall [21].

The blade has a rectangular planform, set at a pitch angle of 9 deg. The section is the S102E airfoil. This is a lifting condition giving a relatively high aerodynamic loading. The reference chord is 0.074 m and the span is 0.185 m, giving an aspect ratio equal to 2.5.

The grid consists of a body-fitted block-structured orthogonal mesh around the airfoil, with 1 million cells and 1,764,000 nodes. A circular block (O grid) is constructed around the airfoil, as shown in Fig. 5. Outer blocks complete the generation of the regular flow

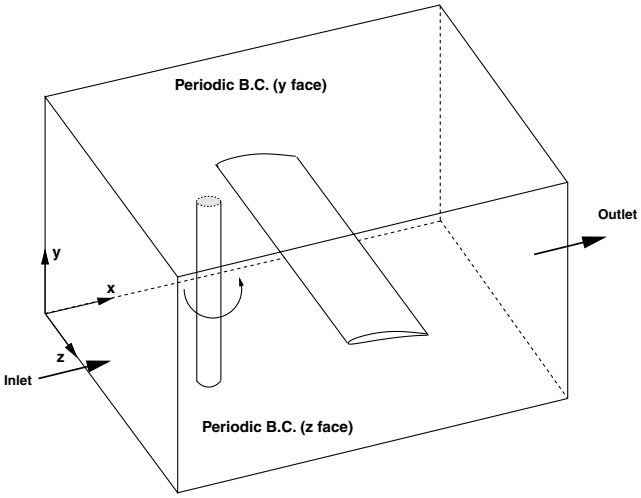

Fig. 4 Integration domain and boundary conditions.

domain. The grid is made of 12 blocks, which are extruded in the spanwise direction. This mesh is considerably more refined than the ones used by Liu and Marshall [21], who also considered low Reynolds numbers ($Re = 2000$ and below), and a nonlifting airfoil section. For this reason, it was deemed appropriate to proceed with this mesh, without specific studies on grid refinement. The domain of integration extended two chord lengths upstream and downstream; it was also two chord lengths above and below the blade. Liu and Marshall investigated the effects of the domain height (in the direction of the vortex axis) and concluded that one blade chord is sufficiently approximate, except in cases where the grid resolution is poor. Therefore, this aspect of the numerics was considered sufficiently resolved.

A single orthogonal vortex was considered. At the starting condition, the vortex was set into a rectilinear flight path. Although the flow environment of the tail rotor is a rotating one, the rectilinear flight path is justified when the convecting velocity of the vortex is much higher than the rotational velocity component of the blade.

The relative velocity $\mathbf{U}_r$ between the convected vortex and the blade is

$$\mathbf{U}_r = \mathbf{U}_v - \Omega\mathbf{r} \tag{8}$$

where $\mathbf{U}_v$ is the convection speed of the vortex, and $\mathbf{r}$ is the radial vector from the rotation point to the vortex core at the impact point. If $\mathbf{U}_v \gg \Omega\mathbf{r}$ (vortex traveling fast against a stationary blade), the planar model is justified. If, instead, the blade rotates fast against a nearly stationary vortex, $\mathbf{U}_v \ll \Omega\mathbf{r}$, then the vortex would tend to follow a curvilinear path on the blade's surface. However, in most cases this rotational effect is believed to be small compared to the viscosity effects after the impact of the vortex.

The vortex strength was assumed to be equal to 4.5. The vortex was assumed to impact the blade at midspan. To introduce a circular vortex into the developed flowfield, the core of the main vortex was assumed to be split into four sections. Within each of these sections, a local velocity field of the same intensity and different directions was introduced. It was ensured through rigorous testing that this procedure would not lead to any instability within the flowfield. However, a side effect of this procedure is that the flowfield shows the presence of two secondary vortices, one ahead of the main vortex and the other behind it. The direction of these vortices in both instances is seen to be opposite to the original vortices. It is speculated that the interaction of the main vortex with the outlying flowfield generates these secondary vortices. These vortices are discussed further in Sec. IV.

In the collocated finite volume approach used, all variables are located at the centers of the cells (which can be of any shape) and the momentum equations are solved by considering an explicit mass flux and upwinding convection schemes. The pressure–velocity coupling is ensured by a prediction/correction method using the SIMPLEC

algorithm. The Poisson equation is solved using a conjugate gradient method. This collocated discretization requires Rhie and Chow's [24] interpolation in the correction step to avoid oscillatory solutions.

The three-time level implicit time advancing scheme (TTLM) of Ferziger and Peric [25] is used for time discretization. This scheme performs the time integration over an interval centered at the new time level and is second order accurate. The nonorthogonalities are taken into account with a reconstruction technique explained by Ferziger and Peric in [25] and are tested for large eddy simulation (LES) by Benhamadouche and Laurence [26]. When a non-orthogonal grid is used, the matrix contains the orthogonal contribution only, and the nonorthogonal part is solved explicitly; this is known as the deferred correction. However, one can iterate on the system to make it quasi implicit. This code has been extensively tested at the University of Manchester on homogeneous grid turbulence, channel flows, and in-line cylinders [27].

The vorticity is calculated as a by-product during the analysis of the data, from the definition $\omega = \nabla \times \mathbf{V}$. The model was closed with Menter's shear-stress transport model for the turbulent shear stresses [28]. This model was chosen because is shows marked improvement in results for complex geometries involving shear layer separation. The model effectively switches between the k–ω in the near-wall region and the k–ϵ model in the far field. On the negative side, the model overpredicts turbulence levels in regions with a large normal strain rate; however, this overprediction is still far less than that of the standard k–ϵ model. However, the model has been used in similar types of problems (see, for example, Geissler et al. [29]).

The oncoming orthogonal vortex travels at a relatively high velocity compared to the domain length, hence to realistically capture any instantaneous effects of the oncoming vortex an extremely small value of time step had to be used; this was 10^{-4} s. The average Courant–Friedrichs–Lewy (CFL) number is 1.5, based on time step and grid resolution.

The solution is started in the unsteady mode without the vortex. The calculation is carried out until the flow is stabilized. Then the vortex is introduced near the inlet section and convected into the field with the inflow velocity.

Because of the size of the mesh, the small time steps required, the need to introduce the vortex when the flow field has been established, the computations are very intensive and required the use of a computer cluster. Processing of the data is also computer intensive, and ultimately not all the flow features could be extracted from the data files.

IV. Results and Discussion

The cases discussed in this study are relative to a vortex intensity $\Gamma = 4.5$, with the rotational velocity of the blade $\Omega = 5600$ rpm (from data taken from a scaled helicopter tail rotor). The direction of rotation is anticlockwise seen from above, as shown in Fig. 2. The inflow velocity is $U = 36$ m/s, corresponding to a Reynolds number $Re = 1.58 \times 10^5$, based on the chord. Along with the Reynolds number, there is the vortex-based Reynolds number, $Re_v = \Gamma/\nu$, which in the present case was $Re_v \simeq 10^5$.

In the first instance, the cases of head-on impact and oblique impact are discussed separately, in order to focus on the vortex dynamics. Then the two cases are considered together, so as to show the different aerodynamic response on the blade (pressure and aerodynamic coefficients). The analysis of the vortex dynamics is best represented by plotting contours of vorticity. For two-dimensional views in the x–y and x–z planes, the vorticity component ω_y (parallel to the undisturbed vortex axis) is the most appropriate component to consider.

A. Straight (Head-On) Impact

Figure 6 shows a time series of the ω_y vorticity contours on the vertical plane through the midspan of the blade. Figure 6a shows the instant when the vortex is impacting the blade and the leading edge. Figure 6b shows the vortex cut around the blade's midsection. The vortex on the suction surface travels faster. The vortex axis is inclined on the vertical axis, but its direction is maintained at a distance from the blade. The analysis of the computational fluid dynamics (CFD) data indicates that the vortex has an axial velocity component in its core.

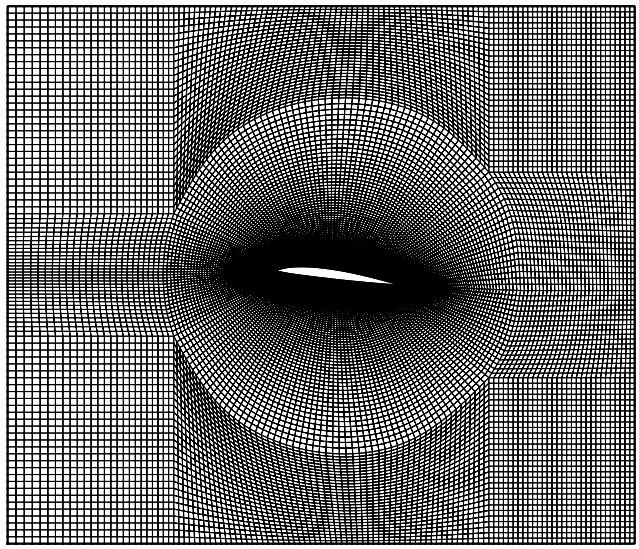

Fig. 5 Mesh topology in the x–y plane.

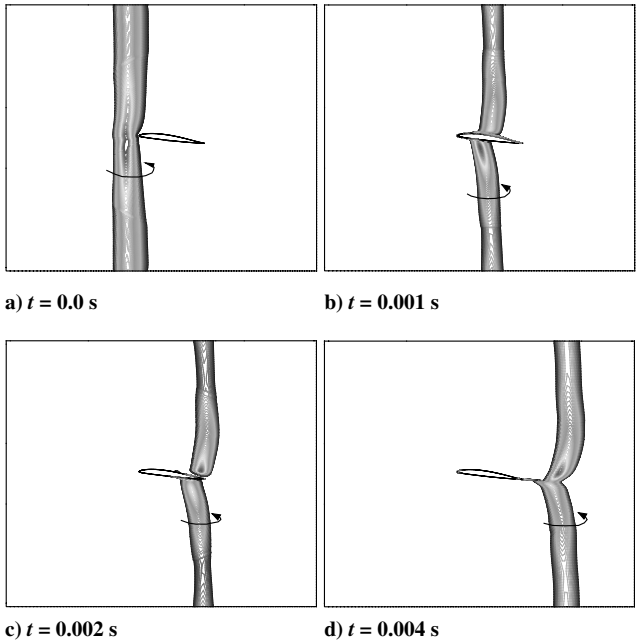

a) t = 0.0 s **b) t = 0.001 s**

c) t = 0.002 s **d) t = 0.004 s**

Fig. 6 Evolution of vortex core in the orthogonal BVI.

Figure 6c shows the vortex in proximity of the trailing edge. In particular, the vortex core on the suction side has just reached the trailing edge, whereas the upper vortex is partially affecting the development of the near wake. Finally, in Fig. 6d the vortex has separated from the blade. There is a strong axial deformation, showing a vortex slowing down in the near wake region, a slight overshoot of the convective speed outside the wake, and a reestablishment of the undisturbed conditions at about one chord away from the blade. This effect is due to the lifting effects of the blade section and is believed to disappears if the blade is symmetric and nonlifting (as demonstrated by Liu and Marshall [21]).

A cut through the center along $x = \text{const}$ and $z = \text{const}$ is shown in Fig. 7, where the normalized axial velocity component v/U_∞ is plotted; "V" is the center of the vortex.

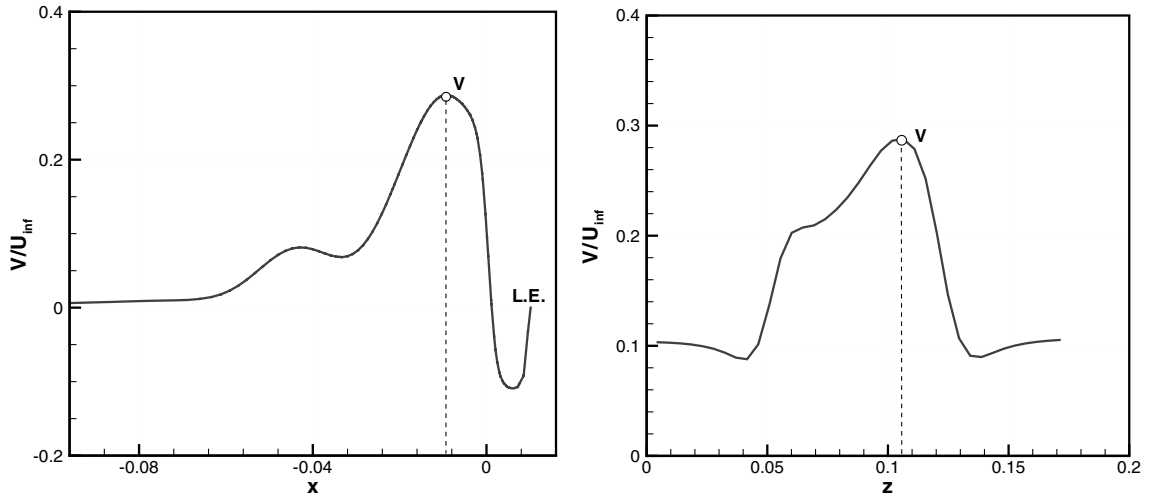

a) $z = 0.1044$ b) $x = -0.0093$

Fig. 7 Axial velocity distribution in the vortex core, case of Fig. 6a.

As explained earlier, the initial condition is $w_o = 0$ (no axial velocity in the vortex core). However, as the vortex is convected downstream an axial velocity component appears, essentially due to self-induced conditions. Analysis of the CFD indicates that the average value $w_o \simeq 2$ m/s at the edge of the core before the impact (Fig. 6a). Hence, the axial flow parameter is $A \simeq 0.7$ as a result of self-induced velocities.

The arrival of the vortex is associated with a region of low pressure ahead, which is of particular interest when it occurs on the blade itself. This is illustrated in Fig. 8. The figure shows regions of high pressure (the maximum is called "H") and low pressure (whose minimum is called "L"). The point V is the approximate position of the vortex core. The plots have been produced at plane cuts $y = \pm 0.009$ or $y/c = \pm 0.122$ (above and below the blade).

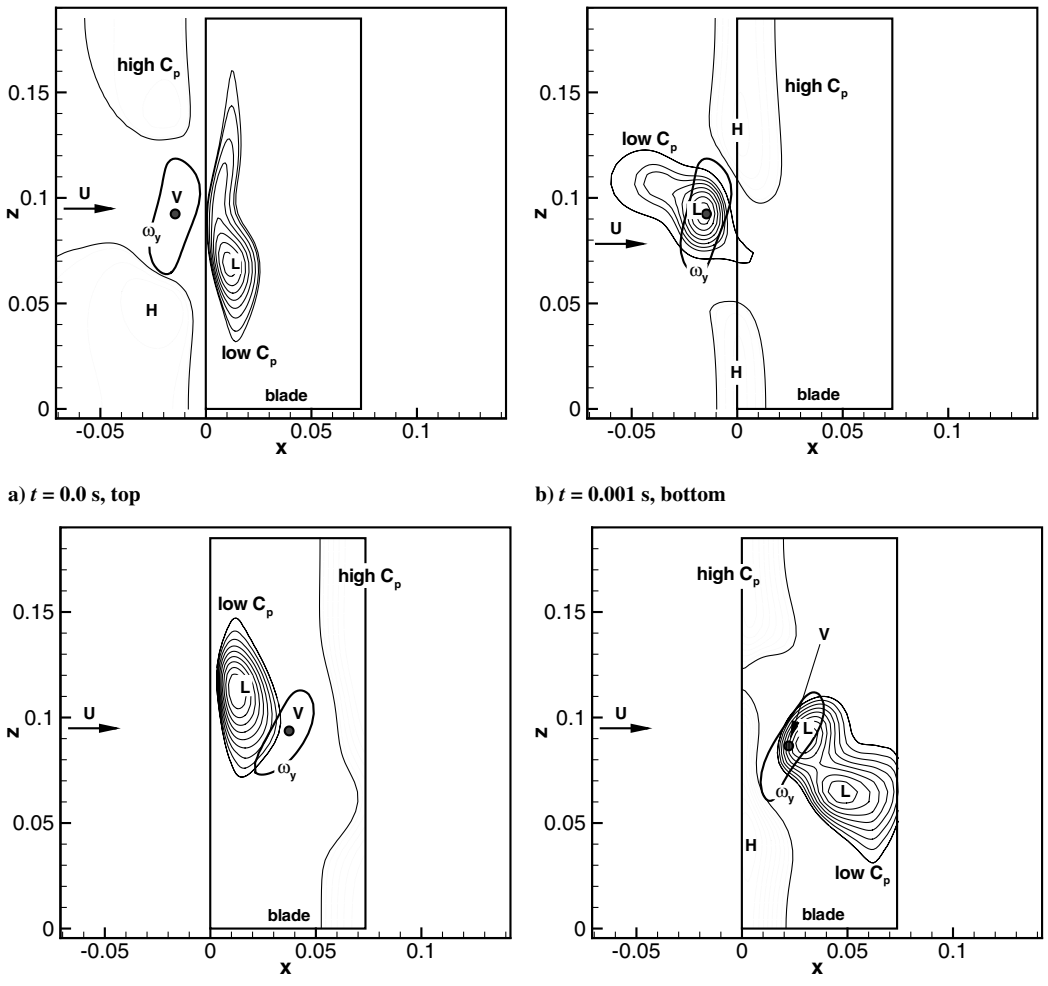

a) $t = 0.0$ s, top b) $t = 0.001$ s, bottom

c) $t = 0.002$ s, top d) $t = 0.004$ s, bottom

Fig. 8 Pressure field and vortex position in straight BVI.

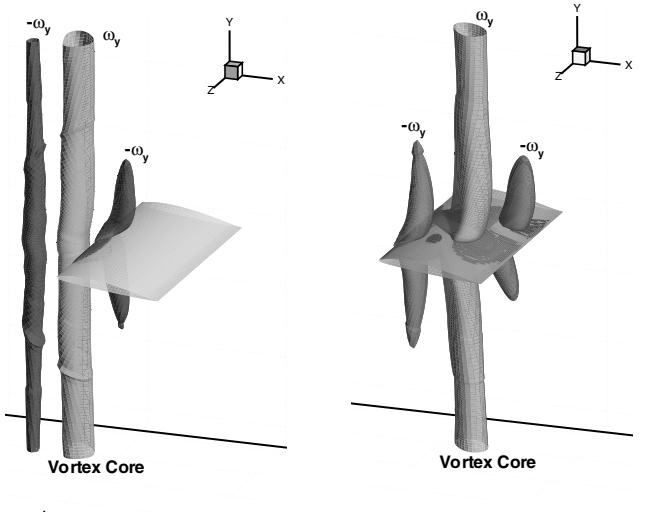

a) $t = 0.0$ s b) $t = 0.001$ s

Fig. 9 Tripolar vortex interaction on the straight BVI.

Because of the extension in the axis direction, and thanks to the spanwise gradients, some instability is to be expected. This instability manifests itself through a deformation of the vortex axis and its core. This phenomenon is not visible from Fig. 6 (which, in fact, shows a well-shaped vortex), but it is found on planes normal to the freestream (y–z planes).

The most striking aspect of this vortex dynamics is the degeneration of the vortex core. The main vortex, in fact, degenerates into a tripolar vortex: the vortex itself and two counter-rotating satellite vortices. One of these vortices is leading the main vortex and the other one is trailing behind. The situation is represented in Fig. 9. This figure shows two isosurfaces of the vertical component of the vorticity, ω_y. The values $\pm\omega_y$ are chosen so as to represent the edge of the primary vortex core as accurately as possible. This strategy allows us to illustrate the relative size of the satellite vortices. It turns out that the leading vortex is relatively short and the trailing vortex is fairly straight, albeit smaller.

The authors are not aware that this effect was identified before. Alternative calculation methods that are currently used for the simulation of the tail rotor BVI are based on potential methods [30]. These methods lack both the resolution and the numerical accuracy for identifying such a phenomenon. Theories are available for the stability of vortex filaments [31,32] and vortex pairs [33,34]. However, these cases do not apply, because the stability or instability of the vortex is disrupted by the BVI event. Also, before the vortex impact the solution is not followed for a long enough time to study the vortex dynamics. The degeneration of a vortex into a tripolar vortex has been identified in the past in fluids with variable density (stratified fluids) and fluids with a strong rotational component (Coriolis effects). However, neither of these effects is present. The effects of numerical diffusion can be identified as a reduction of vorticity (in absolute value), rather than vortex degeneration.

The mechanism of vortex generation is believed to be the following: When the vortex is introduced in the flow field, the vortex-induced velocity is locally oriented against the freestream. This causes the generation of a vortex rotating in the opposite direction. Because the basic vortex core is rotating in the anticlockwise direction (seen from above), a counter-rotating vortex is generated to the left of the basic vortex (seen from upstream). This is illustrated in Fig. 10. If the vortex rotation were in the opposite direction, then the secondary vortex would be on the right side. A similar argument can be proposed for the other secondary vortex, and hence on the tripolar nature of the vortex introduced in the flowfield. The strength, size, and position of these satellite vortices depend on the vortex core, on the circulation Γ, and on the freestream U. These two secondary vortices, although undesirable, were not foreseen. Their evolution is

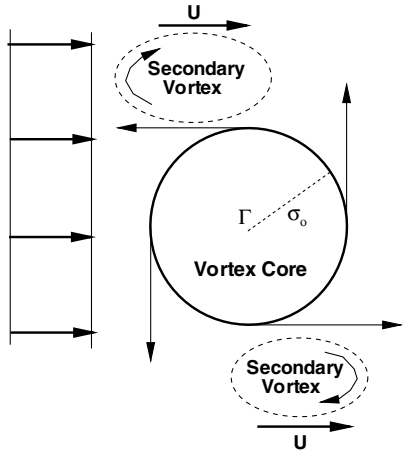

Fig. 10 Mechanism of formation of a secondary vortex.

realistic, based on the introduction of the vortex, and not an effect of the numerical instabilities. However, a full analysis would require a separate study.

Before the vortex impact, a low amplitude wave is seen to propagate away from the impact region, Fig. 9a. The wavelength is estimated at about six vortex core diameters (or three diameters away from the impact point). This problem, similar to the degeneration of the vortex, has seemingly not been identified before and requires a separate study.

B. Oblique Impact (45 degrees)

Figure 11 consists of six frames in the vertical plane through the midspan. This view does not show the spanwise separation between

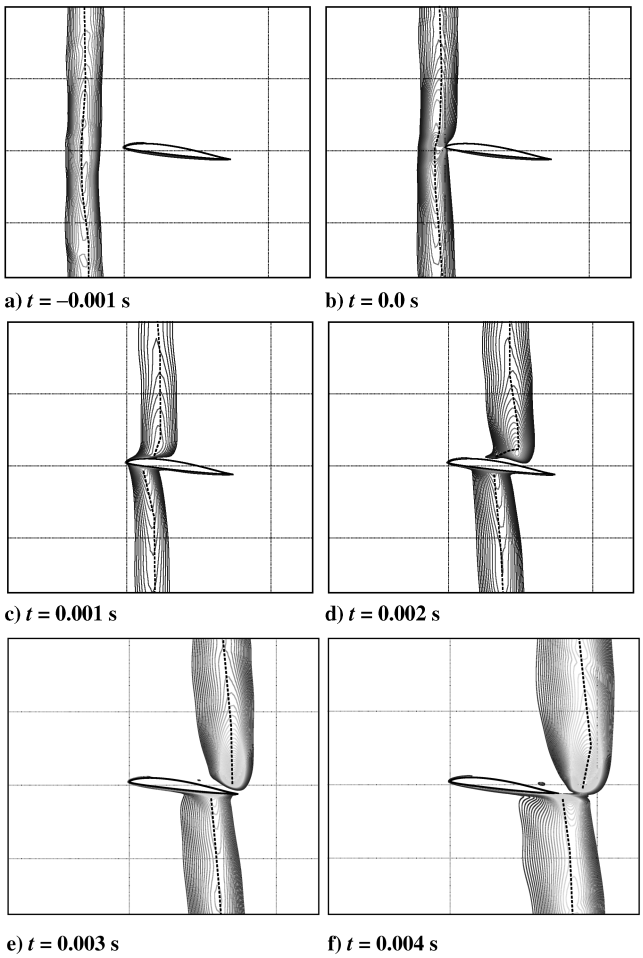

a) $t = -0.001$ s b) $t = 0.0$ s

c) $t = 0.001$ s d) $t = 0.002$ s

e) $t = 0.003$ s f) $t = 0.004$ s

Fig. 11 Vortex core path in oblique BVI on the vertical plane.

the lower and upper vortices. Because the upper and lower vortices travel separately over different paths, this case is discussed separately. The time series includes events from the impact to the departure of the vortex. The dashed line is the estimated center of the vortex. The contour plotted is the vorticity component ω_y (in the direction of the vortex axis). The result shows that the vortex traveling on the upper side (suction side of the blade) separates from the surface of the blade (Figs. 11d and 11e). Also, there is a strong streamwise deformation of the vortex, as a result of its interaction with the slower viscous layer at the surface. In the outer field, where the vortex is not affected by the boundary layer, a further deformation is visible, this time instigated by pressure gradients, which are largely an inviscid problem. It was possible to verify this phenomenon thanks to the extension of the flow domain in the vertical direction. In most cases it is possible to see a layer of vorticity on the pressure side of the blade. This layer interacts with the vortex and affects its deformation. Figures 11d and 11e show an isolated blob of vorticity on the suction side of the blade. In particular, the last frame (Fig. 11f) shows a sizable blob that is interpreted as an isolated vortex with a marked vorticity component along the vertical axis. The orthogonal vortices do not merge completely, because the upper vortex has traveled farther from the trailing edge. However, both vortices interact strongly with the wake. As they are forced to slow down, they also tend to lose strength and expand.

Figure 12 shows the path of the vortex core above and below the blade. For clarity, the position of the leading-edge and trailing-edge lines is shown in the first frame. The two paths diverge when the vortex is cut. The frames indicate the position of the vortex core at distances $z/c = 1,\ 1/2,\ 1/4$, and $1/8$ from the blade, above and below. Shortly after the impact, when the vortex is beginning to split, the two vortex cores travel along different flight paths. These vortices fail to rejoin once they depart from the trailing edge. The dominant parameter, as the graphics in Fig. 12 indicate, is the distance of the vortex core from the blade surface. The leading edge of the blade is placed at $x = 0$. Starting at one chord length above and below the blade, Fig. 12a, the lower vortex core reaches the trailing edge later than the upper vortex. This happens because the point considered is beyond the boundary layer, and as such it is convected downstream without viscous interference from the solid boundaries. As the core gets closer to the blade, the sequence of events is inverted. At $z/c = 1/2$, the vortex "feels" the effects of the solid boundary. The upper vortex is not greatly affected, but the lower vortex at this location travels faster, so that it detaches from the trailing edge sooner than the upper vortex. The phenomenon continues on the same sequence down to $z/c = 1/8$. Note that the path of the vortex is not exactly at 45 deg, which is the direction imposed at the initial condition. The vortex meanders while crossing the blade, although overall it maintains an inclined travel direction with respect to the freestream.

Figures 13 and 14 show the same time series of Fig. 12, this time seen from the front of the blade, on the y–z plane. This view cannot show the streamwise separation between the vortices, and, in fact, the

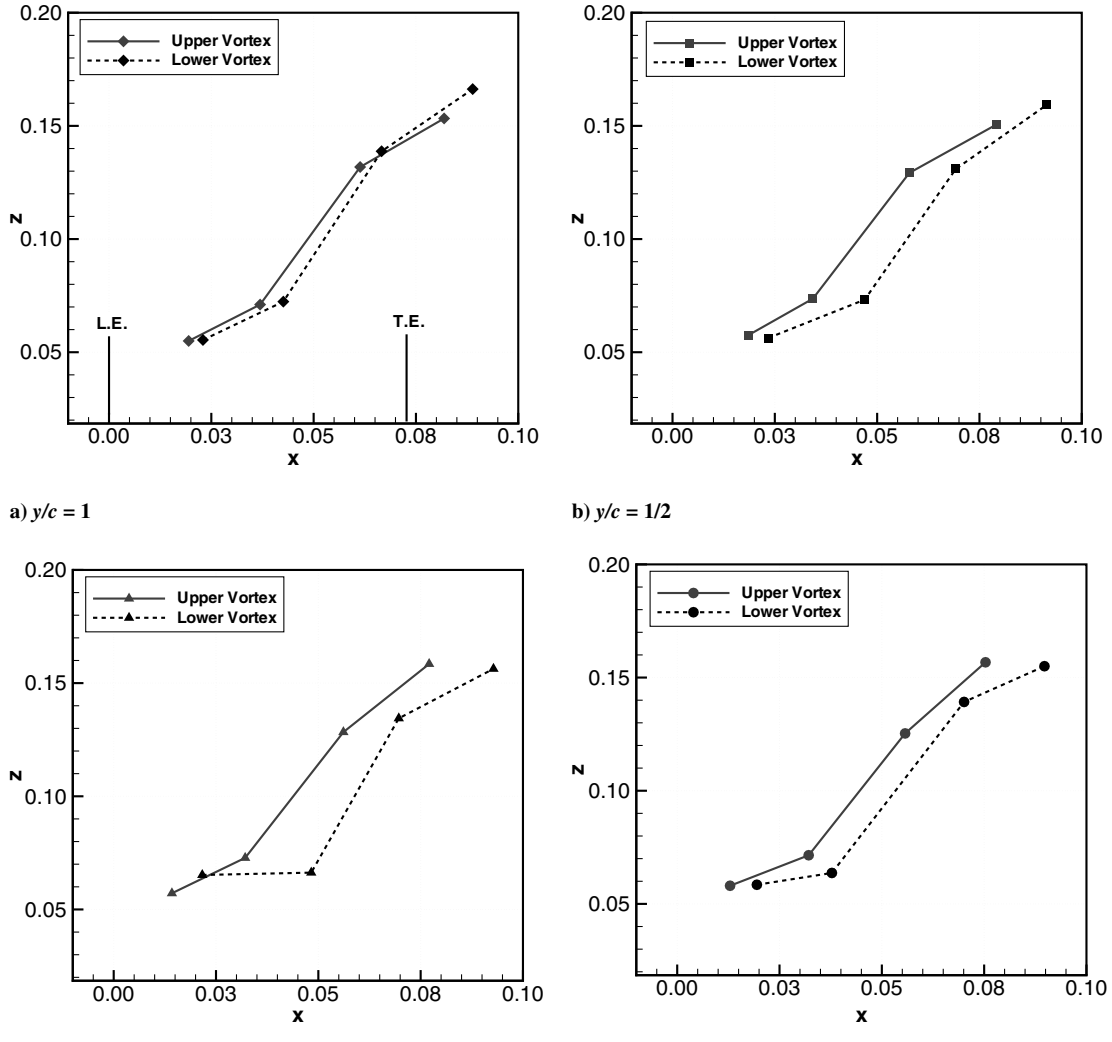

a) $y/c = 1$ b) $y/c = 1/2$

c) $y/c = 1/4$ d) $y/c = 1/8$

Fig. 12 Vortex core path in oblique BVI at selected distances from the blade surface.

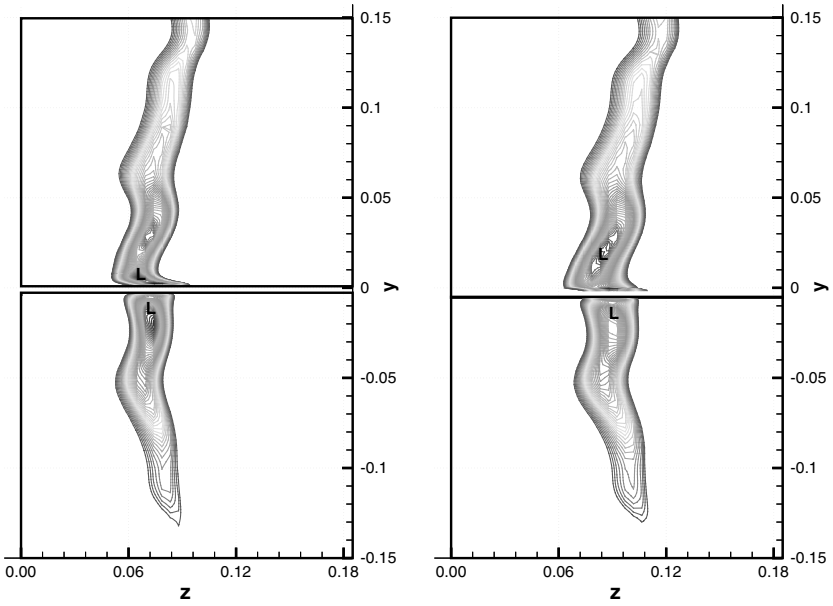

a) x = 0.0318 (top); 0.0452 (bottom) **b) x = 0.0553 (top); 0.0705 (bottom)**

Fig. 13 Vortex core of the oblique BVI on planes y–z, with vortex on the blade.

top and bottom planes shown in each of the frames are shifted (as indicated in the caption), so that they correspond roughly to the vortex core near the blade surface. The main aspect of this result is the leaning of the vortex away from its initial vertical axis. Looking from the front, both vortices lean toward the right of the blade. Once the vortices have passed through the blade, there is a strong interaction with the wake. This is shown in Fig. 13, which is the same time frame as Fig. 12d. The vorticity has been plotted at the planes indicated in the graphs. Along with some instability in the vertical direction, there is a strong shear layer with a spanwise component. At both the fore and aft plane section, Figs. 13a and 13b, respectively, it is noted that the upper and lower vortices have traveled a different spanwise distance. Although reconnection is not possible, because of their streamwise gap, the crosswise gap stretches the wake. The reduction of the vorticity contours is attributed to a dissipation of the vortex away from the wall. Finally, note that on the upper side a secondary vorticity area appears. This is due to a vortex rotating in the opposite direction to the original vortex that trails behind when the original vortex travels across the blade, as described earlier. It is believed that it is generated thanks to the shear created by a combination of vortex core and a velocity gradient around the blade.

C. Comparison Between Straight and Oblique BVI

A direct comparison between the two cases is done in terms of the aerodynamic response of the blade. Figure 15 shows the time-dependent C_p at the midspan section. Figures 15a–15c refer to the lower surface of the blade; Figs. 15d–15f are on the upper surface. The chordwise location is indicated in the graphics. In particular, the analysis was carried out at the leading edge, at one-fourth chord location and at about 60% chord. The time has been normalized with the impact speed and the chord. The C_p range has been maintained constant to illustrate the effect of streamwise position on the magnitude of the pressure changes. All the cases reported show an

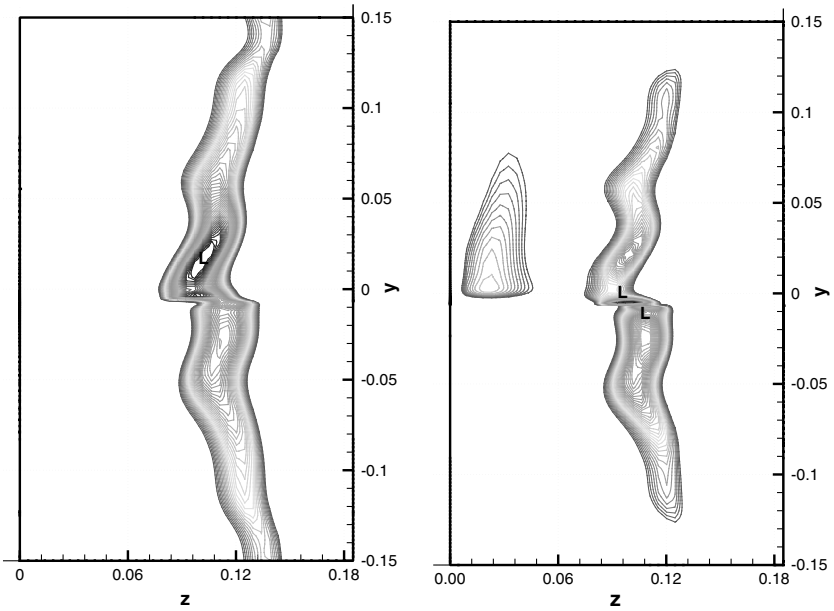

a) x = 0.0775 **b) x = 0.0904**

Fig. 14 Vortex core of the oblique BVI on planes y–z, with vortex past the trailing edge.

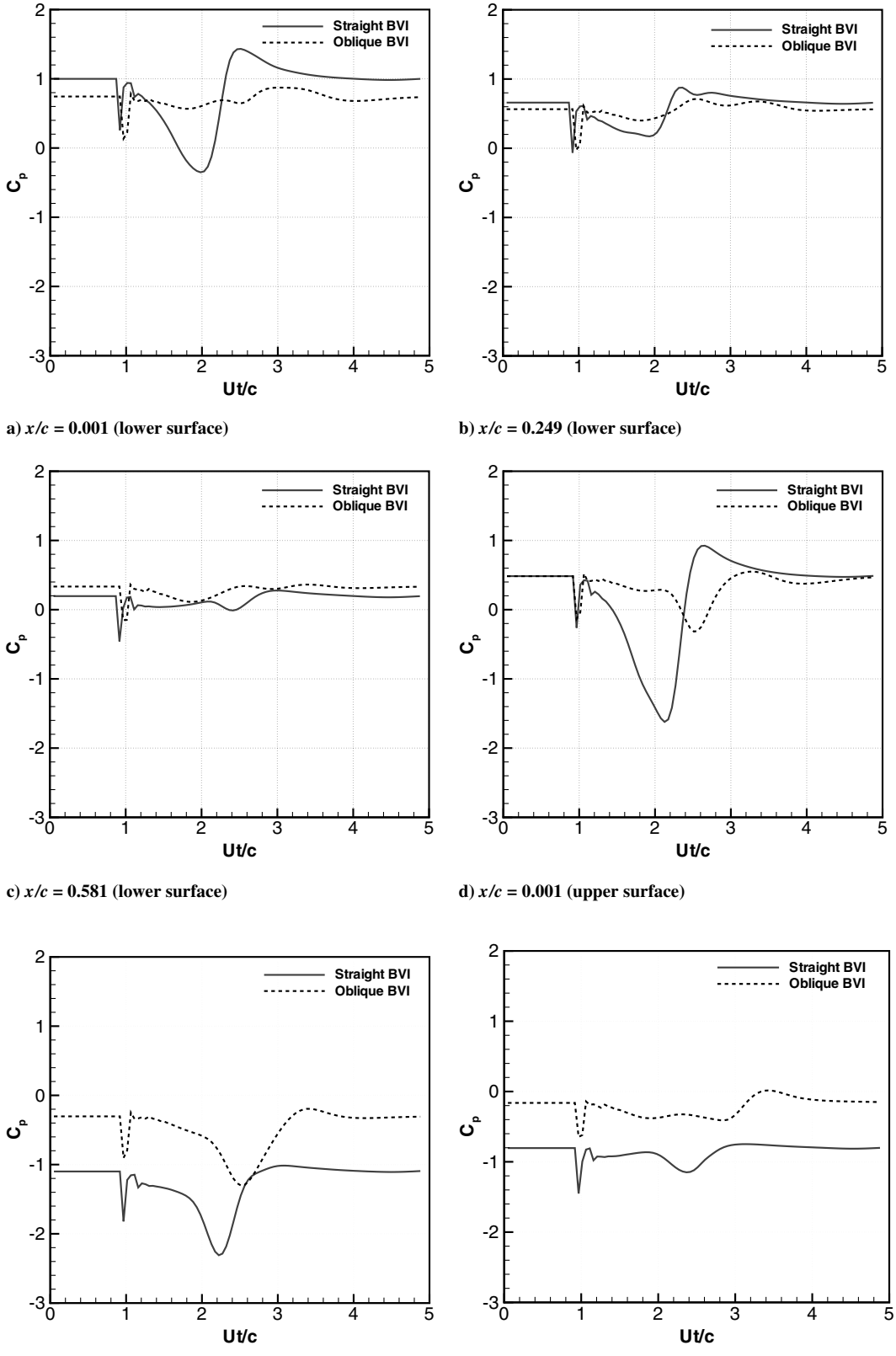

a) $x/c = 0.001$ (lower surface)

b) $x/c = 0.249$ (lower surface)

c) $x/c = 0.581$ (lower surface)

d) $x/c = 0.001$ (upper surface)

e) $x/c = 0.249$ (upper surface)

f) $x/c = 0.581$ (upper surface)

Fig. 15 C_p history at the midspan.

impulsive change in the pressure coefficient, C_p, followed by a damped pressure wave in which the C_p first decreases then increases above the steady-state value. The amplitude of this pressure wave is largest at the leading edge, right after the vortex impact. Downstream (at 60% chord and aft) the amplitude is comparatively small. The difference in C_p level noted in Figs. 15e and 15f is due to the fact that the monitoring station is the same, while the vortex travels along two different paths. The oblique BVI is farther from the monitoring station than the straight BVI. By contrast, when the vortex is at the leading edge, its position is at the midspan, regardless of its path on the blade. Figure 16 shows a three-dimensional plot of the time history of the C_p.

Figure 17 shows the history of the aerodynamic coefficients. The graphs also indicate the position of the vortex core when these

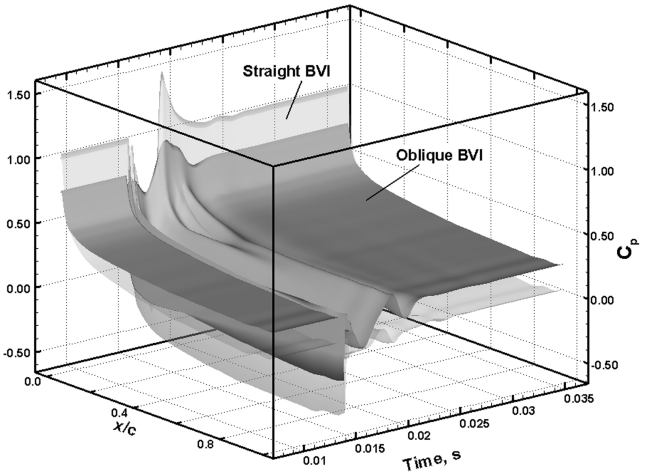

Fig. 16 Time series of the C_p for straight and oblique BVI at the midspan section.

coefficients have a maximum value. The straight and oblique BVI are placed on the same chart to evidence the difference in aerodynamic response. Upon impact, the drag suffers an impulsive increase, followed by an increase in lift. To reach the maximum lift, the vortex has to travel about one-third of the chord after the peak in drag is reached.

The C_L shows a single wave, with a rapid increase in lift and a recovery to the undisturbed level after one damped cycle (a weak secondary wave). The peak in the C_L corresponds to a fully developed vortex lift. The difference in response between the straight and the oblique case is limited to a small difference in the amplitude of the wave and a time shift that can be attributed to the fact that in the oblique BVI the vortex travels at an angle on the blade planform. The C_D suffers a more impulsive peak and a large secondary wave, before eventually recovering to the undisturbed level. Again, the difference between the straight and the oblique BVI is not considerable, but the result indicates a delay in the secondary wave, due to the different flight path of the oblique vortex.

The results published by Wang et al. [14] show the time-dependent normal force coefficient over the steady-state level, $C_n - C_{n_o}$ (relative normal force coefficient). This quantity was also considered by Marshall and Krishnamoorthy [10] to quantify the amount of impulsive loading to the vortex passing, although the comparison is not fully justified. The relative C_n is dependent on the wind speed, on the spanwise section, and on the effective angle of attack of the blade. For a lifting case, the C_n generally decreases before an impulsive rise, as a result of the decreased pressure field ahead of the vortex. Wang et al. do not show a time series long enough to demonstrate that the C_n reaches the undisturbed value once the vortex has passed. Some of the quantities are difficult to measure in the wind tunnel, and, in fact, it is reported that the uncertainty on the vortex circulation is about 35% and the uncertainty on the vortex core radius is as much as 55%. The present case cannot be compared directly with the results of Wang et al., essentially, because of the axial flow parameter, which in the case of the experimental data was $A = 0.54$ at $U = 30$ m/s. Furthermore, the thickness parameter was $t/\sigma_o = 0.486$ (against the present case $t/\sigma_o = 0.165$) and the Reynolds number was 5.67×10^5 (against 1.58×10^5 of the present case). Nevertheless, Fig. 18 shows the impulsive change in the relative C_n, as calculated for the straight and oblique BVI. After the impulsive rise in C_n, the flow is reestablished to the undisturbed conditions, as expected for this case.

An examination of the surface stream traces gives an indication of the effect of the vortex passing on the blade, in particular, the deviation of the flow and the boundary layer separation. Starting from Fig. 19, the stream traces have been plotted on the upper side of the blade. The view includes some vorticity ω_y levels, which had to be derived on a separate plane. In fact, at the solid walls $\omega = \nabla \times \mathbf{U} = 0$, because of the nonslip condition $\mathbf{U} = 0$. Thus, it was decided to cut a plane slightly above or below the blade. These reference planes are at positions $y = \pm 0.0065$, or $y/c = \pm 0.088$. With this operation is it possible to make an approximate reference to the position of the vortex core and to the resulting distribution of

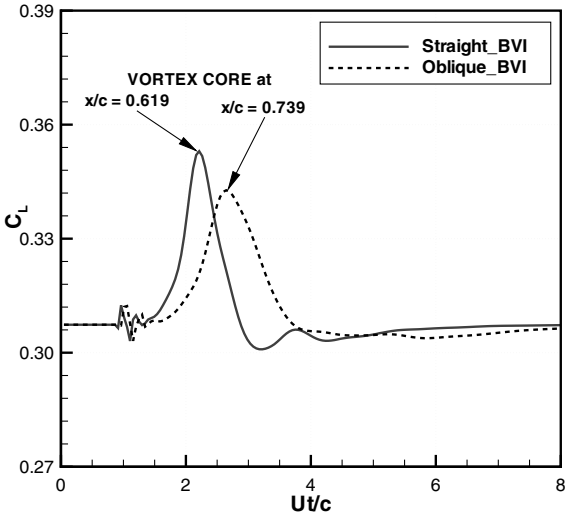

a)

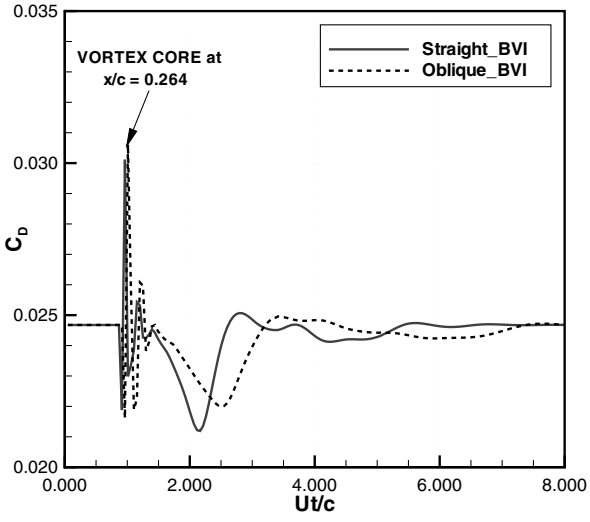

b)

Fig. 17 Blade's C_L and C_D history.

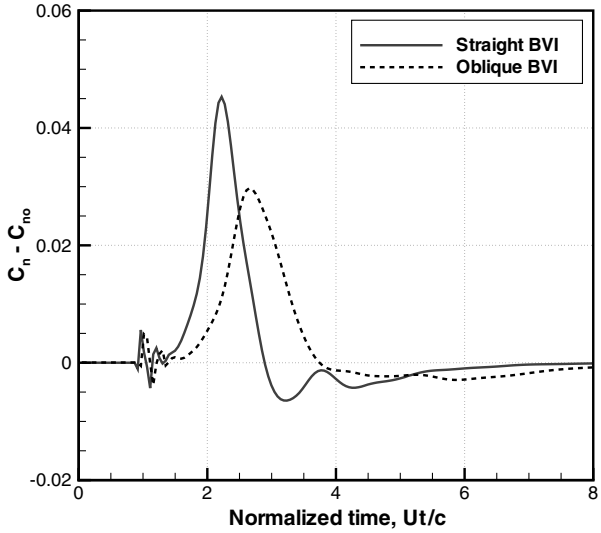

Fig. 18 Blade's residual normal force coefficient.

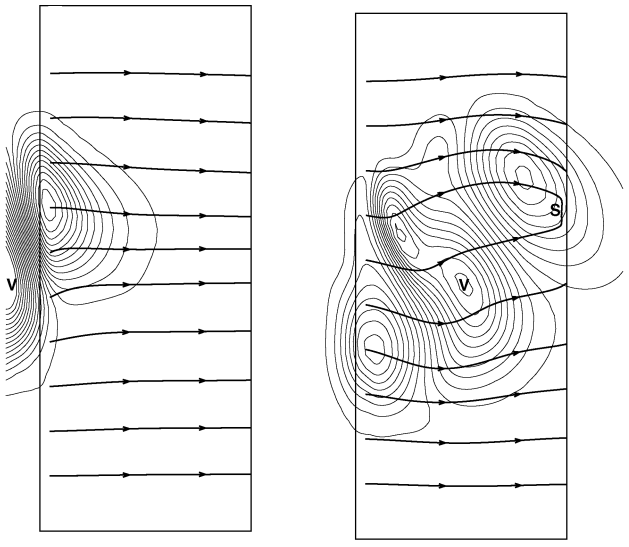

a) $t = 0.0$ s b) $t = 0.001$ s

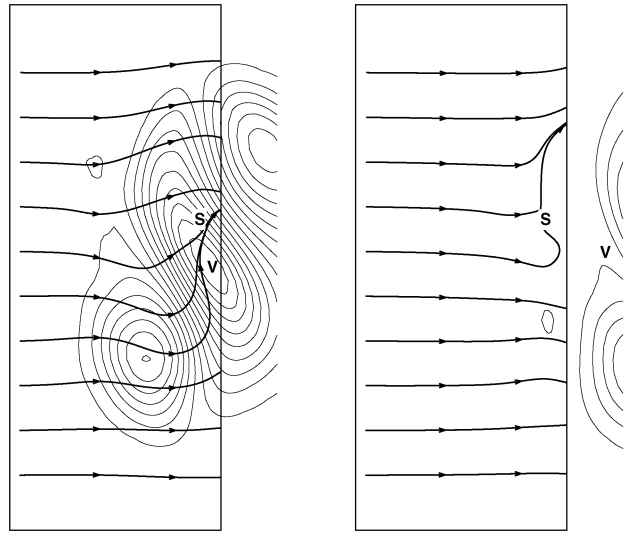

c) $t = 0.002$ s d) $t = 0.004$ s

Fig. 19 Stream traces and ω_y contours for straight BVI, selected time steps (top view).

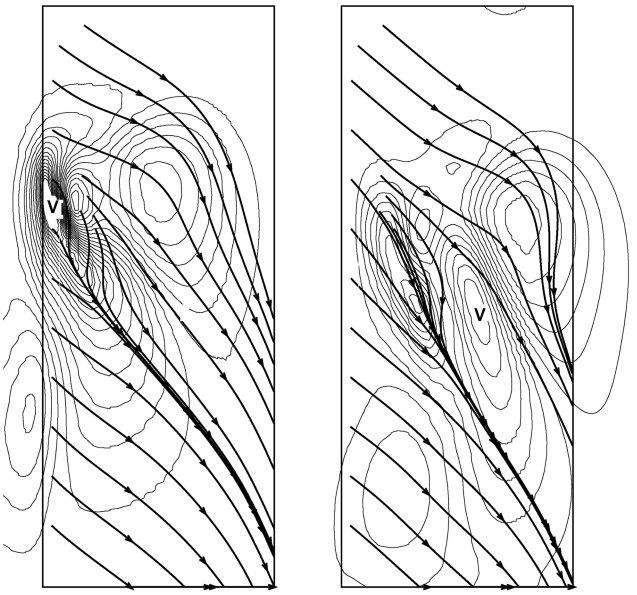

a) $t = 0.001$ s b) $t = 0.002$ s

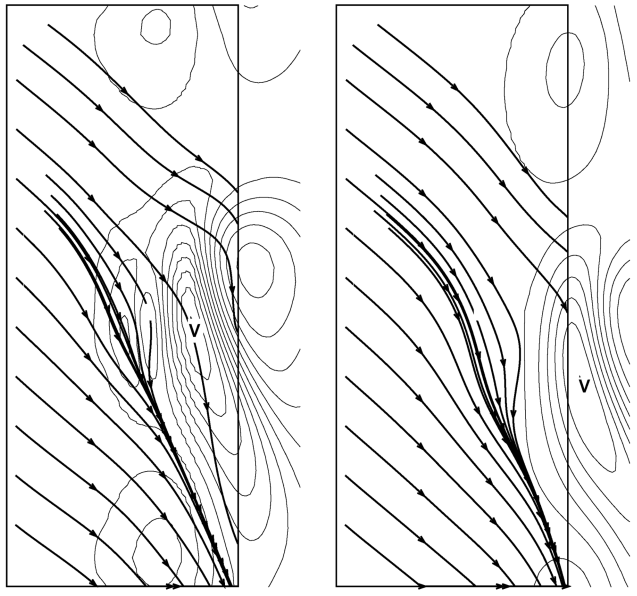

c) $t = 0.003$ s d) $t = 0.004$ s

Fig. 20 Stream traces and ω_y contours for oblique BVI, selected time steps (top view).

vorticity. Figure 19 shows four frames, at the same time steps as indicated in the previous cases (in particular, Fig. 6). The flow is mostly attached, except near the trailing edge, when the vortex is about to pass or has just passed through the blade. Lines of separations are indicated with an "S" in the graphics. In Figs. 19c and 19d the separation appears near the trailing edge before or after the vortex passing. Boundary layer separation precedes the arrival of the vortex core in Fig. 19b, which also shows secondary vortices being created around the wing. Two of these vortices are trailing or leading the main vortex core, and have a vorticity ω_y in the opposite direction, as explained earlier (see also Fig. 10).

Figures 20 and 21 show the stream traces and selected vorticity levels for the oblique BVI, above and below the blade, respectively. In both cases the symbol V denotes the approximate position of the vortex core. The plane cuts are the same as the previous case, for example, $y/c = \pm 0.088$. Therefore, as the vortex travels downstream, its position is tracked on one of these planes, rather than on the blade's surface. For the cases shown in Fig. 20 the blade was rotated by 180 deg. The flow is from the left of the page to the right, as in the view from above. The stream traces have a strong deflection on the blade, particularly in proximity of the vortex core. Boundary layer separation is limited to the presence of the vortex in the middle of the blade, and reattachment occurs as the vortex has passed through the trailing edge, as shown in Fig. 20d.

V. Conclusions

The orthogonal blade-vortex interaction was simulated with an unsteady Reynolds-averaged Navier–Stokes model. The model was based on a planar flow around the outer part of a lifting tail rotor blade. Two cases have been considered: 1) head-on impact at the midspan of the blade, and 2) an oblique impact at the midspan of the blade. It was shown that these cases refer to likely impact directions in the normal operation of a tail rotor blade. The Reynolds number was realistic for the applications discussed.

This study has focused on the vortex dynamics and on the aerodynamic response of the blade upon the impact. The analysis of the data has highlighted a number of physical phenomena. In both cases the vortex is split by the blade. The upper and lower vortices travel at different speeds. In the outer (mostly inviscid) field the vortices are convected by the local pressure, while in the inner viscous field there is a strong interaction between the vortex core and

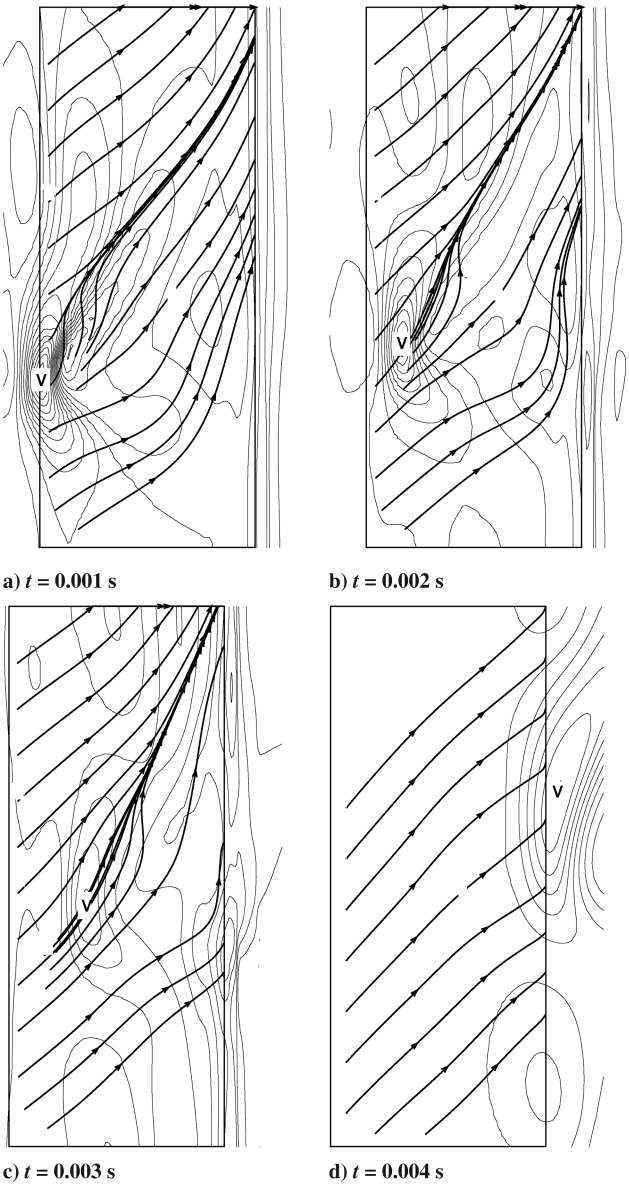

a) $t = 0.001$ s b) $t = 0.002$ s

c) $t = 0.003$ s d) $t = 0.004$ s

Fig. 21 Stream traces and ω_y contours for oblique BVI, selected time steps (bottom view).

the boundary layer. As a result, there is a streamwise stretching of the vortex core that eventually reestablishes a mostly vertical direction. Boundary layer separation only occurs on the aft part of the blade and appears to be localized just upstream of the position of the vortex core. A strong spanwise stretching of the vortex has also been verified, particularly in the oblique case.

Analysis of the spanwise vorticity component indicates that the viscous layer increases in size just downstream of the vortex core. A simple analysis of the axial velocity in the vortex core has been carried out. The results suggest that the axial velocity increases toward the center of the vortex and reaches a maximum at the center. Hence, there is no singularity in the numerical solution, but the result is in contrast with most vortex models (Rankine and similar), and some experimental results.

Because the introduction of a straight vortex core in the flowfield is accompanied by a freestream velocity, secondary counter-rotating vortices are formed around the vortex core before the impact. A basic explanation for these (undesired) vortices has been proposed. The vortices tend to interact with the blade, but the analysis of the unsteady aerodynamic loads does not indicate that they are very effective. The impulsive loads are attributed to the main vortex core. A number of issues regarding the formation and the evolution of these secondary vortices remains unresolved. Another problem that requires further investigation is the nature of the wave traveling along the vortex axis at the BVI impact.

A comparison of the aerodynamic response of the blade in the two cases indicates that the head-on vortex impact causes substantially higher pressure peaks on the suction side. On the other hand, the oblique vortex remains on the blade surface for a longer time, as a result of its path.

A limited set of parameters has been considered in this paper. However, the number of physical parameters involved in the orthogonal BVI, along with the various possibilities regarding the frequency of interaction, the point of interaction, and the rotating effects, make the problem suitable for further study.

Acknowledgments

This research was partly supported by the European Union under the Competitive and Sustainable Growth Programme in the 5th Framework, Contract Number G4RD-CT-2002-00667.

References

[1] Leverton, J. W., Pollard, J. S., and Wills, O. R., "Main Rotor Wake/Tail Rotor Interaction," *Vertica*, Vol. 1, 1977, pp. 213–221.

[2] Cary, C. M., "An Experimental Investigation of the Chopping of Helicopter Main Rotor Tip Vortices by a Tail Rotor. Part 2: High Speed Photography Study," NASA, TR CR-177457, Sept. 1987.

[3] Wittmer, K. S., and Devenport, W. J., "Effects of Perpendicular Blade Vortex Interaction. Part 1: Turbulence Structure and Development," *AIAA Journal*, Vol. 37, No. 7, July 1999, pp. 805–812.

[4] Wittmer, K. S., Devenport, W. J., and Glegg, S. A., "Effects of Perpendicular Blade Vortex Interaction. Part 2: Parameter Study," *AIAA Journal*, Vol. 37, No. 7, July 1999, pp. 813–817.

[5] Leishman, J. G., and Bi, N. P., "Aerodynamic Interactions Between a Rotor and a Fuselage in Forward Flight," *Journal of the American Helicopter Society*, Vol. 35, No. 3, 1990, pp. 22–31.

[6] Bi, N. P., and Leishman, J. G., "Investigation of Rotor Tip Vortex Interactions with a Body," *Journal of Aircraft*, Vol. 30, No. 6, 1993, pp. 879–888.

[7] Affes, H., and Conlisk, A. T., "Model for Rotor Tip Vortex-Airframe Interaction. Part 1: Theory," *AIAA Journal*, Vol. 31, No. 12, Dec. 1993, pp. 2263–2273.

[8] Bhagwat, M. J., and Leishman, J. G., "Generalized Viscous Vortex Model for Application to Free-Vortex Wake and Aeroacoustic Calculations," *Proceedings of the 58th AHS Forum*, American Helicopter Society, Alexandria, VA, June 2002.

[9] Doolan, C. J., Coton, F. N., and Galbraith, R. A., "Surface Pressure Measurements of the Orthogonal Blade Vortex Interaction," *AIAA Journal*, Vol. 38, No. 1, 2001, pp. 88–95.

[10] Marshall, J. S., and Krishnamoorthy, S., "On the Instantaneous Cutting of a Columnar Vortex with a Non-Zero Axial Flow," *Journal of Fluid Mechanics*, Vol. 351, Nov. 1997, pp. 41–74. doi:10.1017/S0022112097007064

[11] Lee, J. A., Burggraf, O. R., and Conlisk, A. T., "On the Impulsive Blocking of a Vortex Jet," *Journal of Fluid Mechanics*, Vol. 369, Aug. 1998, pp. 301–331.

[12] Coton, F., Marshall, J., Galbraith, R., and Green, R., "Helicopter Tail Rotor Blade Vortex Interaction," *Progress in Aerospace Sciences*, Vol. 40, No. 7, 2004, pp. 453–486. doi:10.1016/j.paerosci.2004.11.001

[13] Green, R. B., Doolan, C. J., and Cannon, R. M., "Measurements of the Orthogonal Blade-Vortex Interaction Using a Particle Image Velocimmetry Technique," *Experiments in Fluids*, Vol. 29, Oct. 2000, pp. 369–379. doi:10.1007/s003489900096

[14] Wang, T., Doolan, C. J., Coton, F. N., and Galbraith, R. A., "Experimental Study of the Three-Dimensionality of Orthogonal Blade-Vortex Interaction," *AIAA Journal*, Vol. 40, No. 10, 2002, pp. 2037–2046.

[15] Krishnamoorthy, S., and Marshall, J. S., "Three-Dimensional Blade-Vortex Interaction in the Strong Vortex Regime," *Physics of Fluids*, Vol. 10, No. 11, Nov. 1998, pp. 2828–2845. doi:10.1063/1.869805

[16] Yin, J., and Ahmed, S. R., "Helicopter Main Rotor/Tail Rotor Interaction," *Journal of the American Helicopter Society*, Vol. 45, No. 4, 2000, pp. 293–302.

[17] Marshall, J. S., and Grant, J. R., "Penetration of a Blade into a Vortex Core: Vorticity Response and Unsteady Blade Forces," *Journal of*

Fluid Mechanics, Vol. 306, Jan. 1996, pp. 83–109.

[18] Howe, M. S., "On Unsteady Surface Forces, and Sound Produced by the Normal Chopping of a Rectilinear Vortex," *Journal of Fluid Mechanics*, Vol. 206, Sept. 1989, pp. 131–153. doi:10.1017/S0022112089002259

[19] Marshall, J. S., "Vortex Cutting by a Blade. Part 1: General Theory and a Simple Solution," *AIAA Journal*, Vol. 32, June 1994, pp. 1145–1150.

[20] Marshall, J. S., and Yalamanchili, R., "Vortex Cutting by a Blade. Part 2: Computations of Vortex Response," *AIAA Journal*, Vol. 32, July 1994, pp. 1428–1436.

[21] Liu, X., and Marshall, J. S., "Blade Penetration into a Vortex Core with and Without Axial Flow," *Journal of Fluid Mechanics*, Vol. 519, Nov. 2004, pp. 81–103. doi:10.1017/S0022112004001302

[22] Langer, H. J., Dietrich, O., Oerlemans, S., Schneider, O., and van der Wall, B., "The EU Helinovi Project: Wind Tunnel Investigations for Noise and Vibration Reduction," *Proceeding of the 31th European Rotorcraft Forum*, Sept. 2005.

[23] Lundgren, T. S., and Ashurst, W. T., "Area-Varying Waves on Curved Vortex Tubes with Application to Vortex Breakdown," *Journal of Fluid Mechanics*, Vol. 200, March 1989, pp. 283–307. doi:10.1017/S0022112089000662

[24] Rhie, C. M., and Chow, W. L., "Numerical Study of the Turbulent Flow Past an Isolated Airfoil with Trailing Edge Separation," *AIAA Journal*, Vol. 21, No. 11, 1983, pp. 1525–1532.

[25] Ferziger, J. H., and Peric, M., *Computational Methods for Fluid Dynamics*, 3rd ed., Springer, New York, 2002.

[26] Benhamadouche, S., and Laurence, D., "LES, Coarse LES, and Transient RANS Comparisons on the Flow Across Tube Bundle," *International Journal of Heat and Fluid Flow*, Vol. 24, No. 4, Aug. 2003, pp. 470–479. doi:10.1016/S0142-727X(03)00060-2

[27] Benhamadouche, S., Laurence, D., Jarrin, N., Afgan, I., and Moulinec, C., "Large Eddy Simulation of Flow Across In-Line Tube Bundles," *Proceedings of the 11th International Meeting on Nuclear Reactor Thermal Hydraulics (NURETH)*, Oct. 2005.

[28] Menter, F., "Two-Equation Eddy-Viscosity Turbulence Models for Engineering Applications," *AIAA Journal*, Vol. 32, No. 8, Aug. 1994, pp. 1598–1605.

[29] Geissler, W., Dietz, G., and Mai, H., "Dynamic Stall on a Supercritical Airfoil," *Aerospace Science and Technology*, Vol. 9, No. 5, July 2005, pp. 390–399. doi:10.1016/j.ast.2005.01.012

[30] Gennaretti, M., and Bernardini, G., "Novel Boundary Integral Formulation for Blade-Vortex Interaction Aerodynamics of Helicopter Rotors," *AIAA Journal*, Vol. 45, No. 6, June 2007, pp. 1169–1176. doi:10.2514/1.18383

[31] Moore, D. W., and Saffman, P. G., "The Instability of a Straight Vortex Filament in a Strain Field," *Proceedings of the Royal Society of London, Series A: Mathematical and Physical Sciences*, Vol. 346, Nov. 1975, pp. 413–425. doi:10.1098/rspa.1975.0183

[32] Tsai, C. Y., and Widnall, S. E., "The Stability of Short Waves on a Straight Vortex Filament in a Weak Externally Imposed Strain Field," *Journal of Fluid Mechanics*, Vol. 73, No. 4, Feb. 1976, pp. 721–733. doi:10.1017/S0022112076001584

[33] Crow, S. C., "Stability Theory for a Pair of Trailing Vortices," *AIAA Journal*, Vol. 8, No. 12, Dec. 1970, pp. 2172–2179.

[34] Fabre, D., Cossu, C., and Jacquin, L., "Spatio-Temporal Development of the Long and Short-Wave Vortex-Pair Instabilities," *Physics of Fluids*, Vol. 12, No. 5, May 2000, pp. 1247–1250. doi:10.1063/1.870375

R. So
Associate Editor